Heliyon 6 (2020) e04568

Contents lists available at ScienceDirect

Heliyon

journal homepage: www.cell.com/heliyon

Research article

Graphene oxide based coconut shell waste: synthesis by modified Hummers method and characterization

E.H. Sujiono [a,*], Zurnansyah [a], D. Zabrian [a], M.Y. Dahlan [a], B.D. Amin [a], Samnur [b], J. Agus [c]

[a] Laboratory of Materials Physics, Department of Physics, Universitas Negeri Makassar, Makassar, 90224, Indonesia
[b] Department of Mechanical Engineering, Universitas Negeri Makassar, Makassar, 90224, Indonesia
[c] Department of Physics, Faculty of Science and Technology, Universitas Islam Negeri Alauddin Makassar, Makassar, 92113, Indonesia

ARTICLE INFO

Keywords:
Materials science
Materials chemistry
Organic chemistry
Nanotechnology
Coconut shell waste
Graphene oxide
Band gap energy

ABSTRACT

Graphene oxide (GO) based on coconut shell waste was successfully synthesized using a modified Hummers method, and the obtained GO was confirmed using XRD, FTIR, Raman spectroscopy, UV-Vis spectroscopy, and SEM-EDX. The XRD spectroscopy obtained the fractional content of the 2H graphite phase of 71.53%, 14.47% phosphorus, 10.02% calcium, and 3.97% potassium in coconut shell charcoal, where the GO sample tend to forms a phase of reduced graphene oxide (rGO). FTIR spectra shows compound functional groups of hydroxyl (- OH) at peak 1 (3449.92 cm^{-1}), carboxyl (-COOH) at peak 2 (1719.42 cm^{-1}) and peak 3 (1702.62 cm^{-1}), and alcohol (C–OH) at peak 4 (1628.12 cm^{-1}) and epoxy (CO) at peak 5 (1158.51 cm^{-1}), which is similar to the GO synthesis from pure graphite. Raman spectroscopy analysis shows that the value of the I_D/I_G intensity ratio of the GO sample was 0.89 with a 2D single layer, and SEM results showed that surface morphology with an abundance of granular particles were found with different size distribution. The UV-visible results showed sufficient optical properties characterized by the spectrum, which formed because of the light absorption of the energy passed on the sample. The bandgap energy value of the sample obtained by the Tauc plot method was 4.38 eV, which indicates semiconductor properties.

1. Introduction

Graphene is an exciting material that has an uncommon two-dimensional skeleton with a hexagonal structure of single monomolecular layer of sp2-hybridized carbon atoms [1, 2]. Graphene has attracted intense interest in the many areas of science and technology because of its unique properties [3] such as excellent electronic [4, 5, 6], thermodynamic, and mechanical properties [7, 8]. Graphene has a wide range of applications such as transparent conductive films, field effect transistors (FET), water purification, energy storage devices, and sensors due to its outstanding physical and chemical properties [9, 10, 11, 12, 13]. The first fabrication of single-layer graphene nanosheets was achieved by an exfoliation technique called the Scotch-tape method from bulk graphite [14] and by epitaxial chemical vapor deposition. However, the drawback of these methods is that they are not applicable for graphene manufacturing in industrial production [15]. Synthesis of graphene nanosheet using mechanical exfoliation method is not applicable for large scale production. Therefore, the development of large-scale synthesis methods from materials that are structurally similar to graphene has attracted increasing research attention [16]. One of the most prevalent and interesting approaches for graphite exfoliation on a large scale is through the use of active oxidizing agents in a chemical reaction to produce graphene oxide (GO) which is a carbon material with nonconductive hydrophilic properties [17].

GO is a carbon material that shows chemical, optical, and electrical properties similar to those of graphene because it is based on the graphene framework [18]. However, GO differs from graphene in that oxygen functional groups such as epoxy and oxygen groups are located on the basal plane of GO, and small amounts of carbonyl and carboxyl groups are present at its sheet edges [19, 20, 21]. GO can be synthesized by several methods [22]; the Brodie method reported in 1859 was the first method where fuming HNO_3 and $KClO_3$ are used as the intercalation agent and oxidant, respectively [1]. In 1958, Hummers and Offerman developed a method for the synthesis of GO [23]. This method uses H_2SO_4 to exfoliate graphite with $NaNO_3$ and $KMnO_4$ as the oxidizing agents of graphite. The Hummers method has some advantages compared to the method of Brodie and Staudenmaier. First, KMnO4 as a strong oxidant helps to accelerate the reaction so that the synthesis can

* Corresponding author.
E-mail address: e.h.sujiono@unm.ac.id (E.H. Sujiono).

https://doi.org/10.1016/j.heliyon.2020.e04568
Received 13 November 2019; Received in revised form 24 February 2020; Accepted 23 July 2020

be achieved in a few hours. Second, chlorate is not used eliminating the possibility of ClO2 explosion. Third, the substitution of fumigation with NaNO3 removes the acid mist produced by HNO3. Therefore, this method can be an effective approach for producing GO on a large scale [24].

Graphite powder is the primary precursor for GO synthesis [25]. Graphite is found in nature in three forms, namely, as amorphous (70–80%), crystalline flakes (90–98%), and crystalline lumps or veins (90–99%) [26]. Graphite is classified into natural graphite and synthetic graphite that can be produced by graphitization utilizing heat-induced of hydrocarbon precursors [27]. In nature, one of the materials that contain hydrocarbon compounds is coconut shell charcoal [28] that has a high carbon content of 74.3% [29]. Several methods have been reported for the graphitization of natural materials such as pyrolysis, template method, foaming technique, catalytic graphitization [30].

In this study, GO was synthesized based on the graphite produced from the coconut shell waste by a modified Hummers method. Meanwhile, graphite powder was obtained by the graphitization of the coconut shell using the pyrolysis method. These methods are facile and are suitable for low-cost fabrication [31]. The samples were characterized by X-ray diffraction (XRD), Fourier Transform infrared (FTIR), Raman spectroscopy, UV-Vis spectroscopy, and scanning electron microscopy-energy dispersive X-ray (SEM-EDX) to confirm the GO.

2. Experimental procedure

2.1. Fabrication of graphite powder

Coconut shell was obtained from Bone Regency in South Sulawesi, Indonesia. The raw material was washed and cleaned from the husk, and then was dried by solar thermal treatment for three days. The sample was crushed into granular particles with the size of 2–3 mm and labelled as CSBM. The sample was carbonized at 600 °C for 3 h to produce high-carbon coconut shell charcoal [32]. The sample was ground, and sieved to obtain a powder with a particle size of 75 μm using a 200 mesh siever. Then, the sample was washed with 40% hydrofluoric acid (HF) to remove the impurity compounds [33, 34], and stirred with the sample to acid ratio of1:3 while maintained at 45 °C for 3 h. Then, the solution was washed with deionized water and NaOH until reaching pH of 6–7 and was dried in an oven at 110 °C for 12 h. The obtained graphite powder was characterized by XRD to obtain the phase composition of the sample.

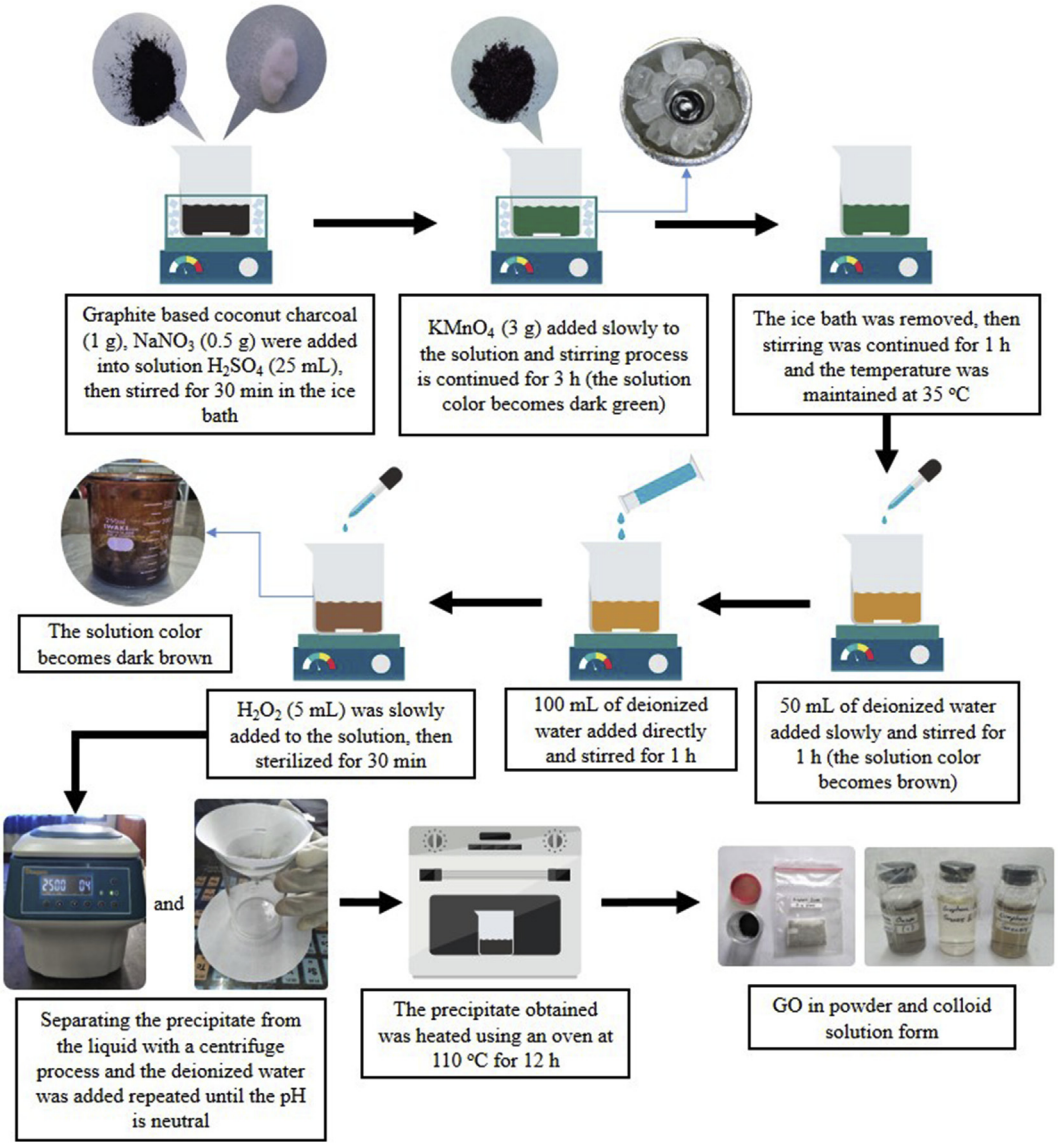

Figure 1. Schematic of GO synthesis by a modified Hummers method.

2.2. Synthesis of GO by modified Hummers method

The GO sample was synthesized by a modified Hummers method. The following was used: graphite-based coconut charcoal (1 g) and $NaNO_3$ (0.5 g) was mixed into H_2SO_4 (25 mL) and then stirred for 30 min in an ice bath. After the stirring process, $KMnO_4$ (3 g) was added slowly to the solution, and the stirring was continued for 3 h until the solution colour became dark green. During the stirring process, the temperature was maintained in the range of 20-0 °C in an ice bath. The solution was removed from the ice bath, and then stirring was continued for 1 h, while the temperature was maintained at 35 °C. Subsequently, deionized water (50 mL) was slowly added and the solution was stirred for 1 h.

Then, deionized water (100 mL) was directly added again and sterilized for 1 h. In the next step, hydrogen peroxide (H_2O_2) (5 mL) was slowly added to the solution and then sterilized for 30 min to remove the excess of KMnO4. After this process, centrifugation was performed to separate the precipitate from the liquid, and the deionized water was added until neutral pH was reached. The obtained precipitate was heated using an oven at 110 °C for 12 h to produce GO powder. The GO synthesis by the modified Hummers method is schematically illustrated in Figure 1.

2.3. Characterization

X-ray diffraction analysis was performed using a Shimadzu XRD 7000 diffractometer (Shimadzu, Japan) with an acceleration voltage of 40 kV and current of 30 mA. The intensity data collected in the ranges of 10–55°and 0–65°for graphite and GO, respectively, using a step scan mode. The elemental composition was analysed using Match! Match! is used to carry out semiquantitative analysis in order to identify the phases of the sample diffraction data by comparing the diffraction pattern of the sample with a database containing the diffraction patterns as reference information. Therefore, sample information such as phases and elements can be easily applied. FTIR spectroscopy was performed using a Thermo Scientific Nicolet iS10 instrument in the 4000-500 cm-1 range using KBr pellets to identify functional groups of the GO. A Raman spectrometer (Horiba Jobin-Yvon LabRam HR800) was used to detect the ordered and disordered crystalline structures and to distinguish between the single and multilayer GO. Scanning electron microscopy-energy dispersive X-ray (SEM-EDX) characterization was performed using an FEI Inspect S50 instrument with the samples placed on the holder and then coated by Au–Pd to obtain the surface morphology and elemental percentage of the GO. The optical characterization was performed by UV–Vis spectroscopy (Cary 50 UV-Vis Spectrophotometer from Agilent Technologies) at room temperature in the colloidal solution form in a UV Quartz cuvette with a path length of 1 cm.

3. Results and discussion

GO-based graphite powder from coconut shell waste was successfully produced by the modified Hummers method. The GO sample was obtained in two forms, as powder and as a colloid solution. The powder sample was characterized using SEM-EDX, XRD, FTIR, and Raman spectroscopy, while the colloid solution sample was characterized by UV-Visible spectroscopy.

3.1. Scanning electron microscopy-energy dispersive X-ray analysis

The SEM image shows the surface morphology of the GO sample given in Figure 2. It is clear from Figure 2 that the GO sample surface has an abundance of granular particles and contains pores with different sizes. As shown in Figure 2(a), the GO sample at the scale of 100 μm displays particles with different sizes ranging from 4.26 μm to 47 μm with the pore size of 2.71 μm. From Figure 2(b), it is observed that the GO sample at the scale of 10 μm has particles size ranging from 0.76 μm to 10.47 μm, where as Figure 2(c) for the GO sample with the scale of 5 μm

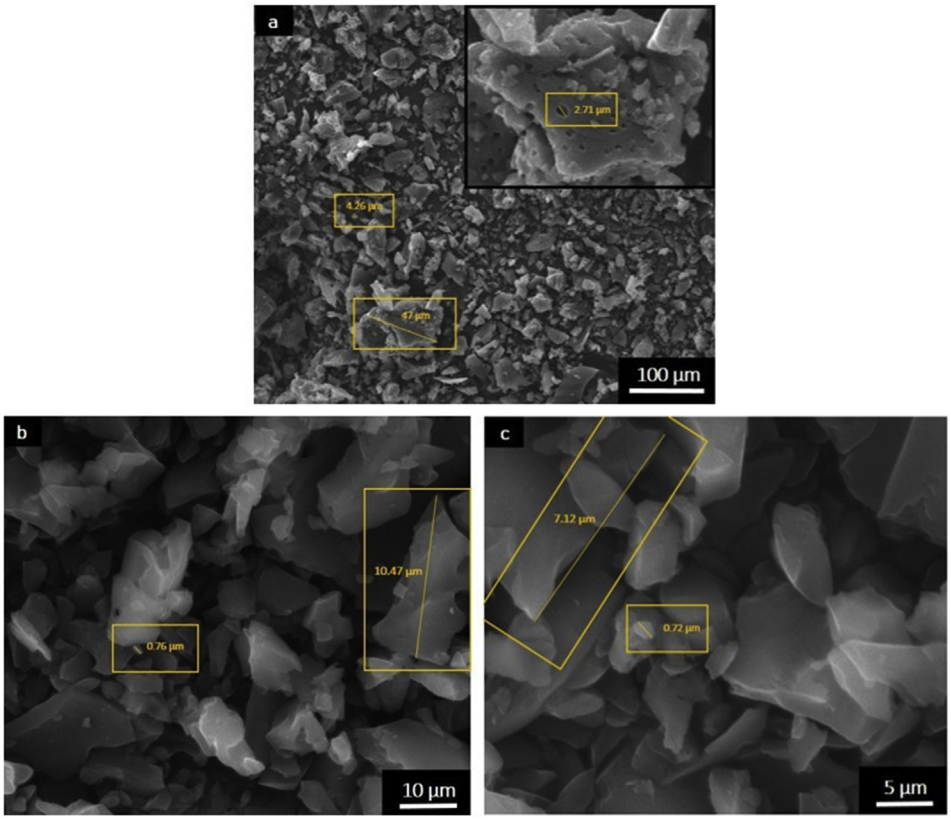

Figure 2. SEM image of the GO samples based on coconut shell waste, a) with scale 100 μm, b) 10 μm and c) 5 μm.

contains particles with the sizes ranging from 0.72 μm to 7.12 μm. The differences in the grain size can affect the mechanical properties of the material [35]. As the grain size decreases, then Young's modulus and fracture strength decrease while fracture strain increases [36]. Therefore, this material is highly promising for use as a polymer matrix to create advanced multifunctional composites with potential application in aerospace, automobile and defence industries [37]. Kittiratanawasin and Hannongbua (2016) showed that size, edge, and shape of graphene can affect the bandgap and used the atomistic tight-binding method to compute the bandgap energies of graphene lattices (quantum dot) with hexagonal, triangular, rectangular and parallelogram shapes with zigzag and armchair edges [38].

The EDX results obtained for the GO sample are shown in Figure 3, where the highest peak was obtained for carbon with oxygen and sulfur as the impurities. The impurities that are observed in the EDX results do not appear in the XRD GO results because XRD characterizes the material by analysing the crystal structure and comparing it against a database of known structures. However, XRD has a weak capability for detecting amorphous materials in the sample. Moreover, compared to XRD, EDX experiments require very little materials science expertise less initial information regarding the samples. EDX is usually combined with scanning electron microscopy, making it a multipurpose device for obtaining a map of the sample composition or for performing area-specific elemental analysis. Further information about the EDX results from the GO sample is provided in Table 1.

Table 1. EDX element result of the GO sample.

Element	Wt %	At %
CK	80.01	84.69
OK	18.54	14.73
SK	01.45	00.58

3.2. X-ray diffraction analysis

Figure 4 shows the diffractogram patterns from the XRD characterization results that obtained information about the elemental content fraction and phases formed in the coconut shell charcoal after washing with hydrofluoric acid (HF). The presence of the amorphous phase of the sample is due to the use of raw materials obtained from natural resources. The results of analysis performed using Match! are shown in Table 2. The identification of a high graphite phase in the carbon element indicates the excellent graphitization process from coconut shell waste [31], and other elemental impurities in the sample were present because the washing process was not optimal [39] and coconut shell contains soil macronutrients such as carbon (C), oxygen (O), hydrogen (H), nitrogen (N), phosphorus (P), potassium (K), sodium (Na), calcium (Ca) and magnesium (Mg) [40, 41].

Using the data presented in Table 3, the microstructure was obtained from the 2θ data, intensity and FWHM (Full-Width at Half Maximum) that were interpreted based on the three highest elemental peaks in the graphite material based on coconut shell waste. The first highest peak is shown by element C (Graphite 2H) at 2θof 44.0462° with intensity of 1312 cps and an FWHM value of 0.18530°. The second highest peak was obtained for the K element (potassium) at 2θ of 39.5240° with intensity of 395 cps and the FWHM value of 0.15370°, while the third-highest peak

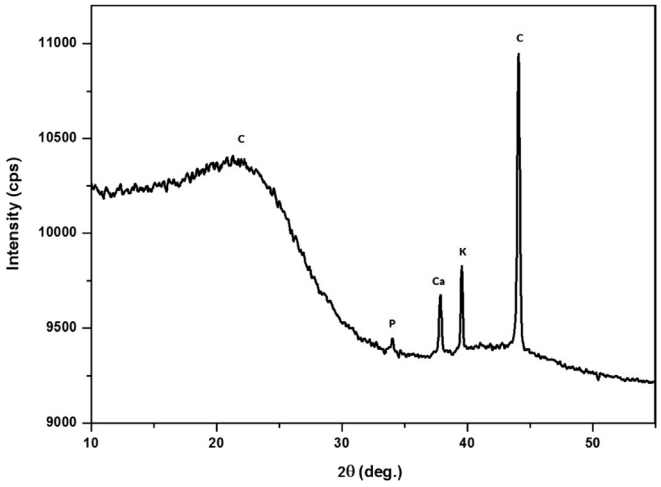

Figure 4. XRD diffractogram pattern with elemental content in coconut shell charcoal after washing with hydrofluoric acid (HF).

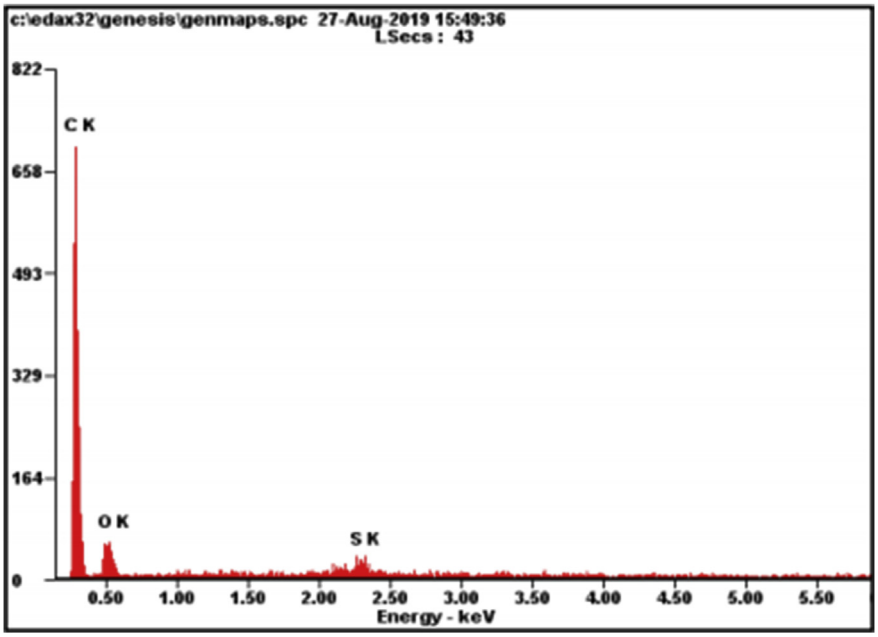

Figure 3. EDX result of the GO-based on coconut shell waste.

Table 2. Match! analysis result of graphite-based on coconut shell waste.

Formula	Legend	%
Carbon Graphite 2H	C	71.53
Calcium-beta	Ca	10.02
Phosphorus – black	P	14.47
Potassium	K	3.97

was found for Ca (Calcium-beta) at of 2θ of 37.8129° with intensity 258 cps and FWHM value of 0.19240°. These FWHM values indicate the homogeneity of the crystal in the sample because a smaller FWHM value corresponds to a homogeneous lattice or crystal structure implying a higher material quality [42].

The XRD diffractogram pattern of GO in Figure 5 shows its amorphous structure but nevertheless exhibits two dominant peaks at 2θ of 23.97° and 43.04°. These peaks tend to indicate that the sample contains a reduced Graphene Oxide (rGO) phase [43, 44, 45]. The shift in the diffraction pattern of the GO material which is typical of the formation of rGO may be due to two effect; first, because the precursor used in the synthesis is an amorphous material [29], and second, because of the changes in the oxidation degree that occur during the synthesis process. Graphite has a high oxidation rate, but some samples were reduced during the drying process in an oven such that the groups of oxygen compounds were separated from the GO bonding layer [43].

3.3. Fourier Transform infrared analysis

The results of FTIR spectroscopy measurements are shown in the form of a peaks interactions graph of each molecule in the sample that absorbs energy from the infrared part of the electromagnetic wave spectrum; this is shown by the figure of the relationship between the percentage of transmission (%T) and the wave number (cm^{-1}) [46]. FTIR spectroscopy was performed to investigate the functional groups of GO [47].

Figure 6 shows the position of the absorption peaks of GO in the FTIR spectrum that indicates that different functional groups have different bond energies [48]. Stretching vibrations from hydroxyl groups (-OH) in water molecules (-OH) gave rise to peak 1 (3449.92 cm^{-1}) [49], carboxyl (-COOH) vibrations gave rise to peak 2 (1719.42 cm^{-1}) and peak 3 (1702.62 cm^{-1}) [22], alcohol (C–OH) vibration gave rise to peak 4 (1628.12 cm^{-1}) and epoxy (C–O) vibrations at peak 5 (1158.51 cm^{-1}) were also observed [46, 50]. Thus, the FTIR spectroscopy results confirmed the appearance of various oxygen-containing functional groups such as hydroxyl, carboxyl, alcohol, and epoxy within the GO structure and were similarities to the FTIR spectrum for GO reported by Xu *et al.*, (2017). A comparison of the functional groups between the GO-based coconut shell waste with the GO reported from Xu *et al.* (2017), who synthesized GO from commercial graphite, is shown in Table 4.

3.4. Raman spectroscopy analysis

Raman spectroscopy is an effective technique for the observation of carbonaceous materials include graphene and GO. It can also be applied to detect organized and disorganized crystalline structures and to identify the single or multilayer properties of the GO sample [27, 51]. Structural changes that occur during the chemical conversion from graphite to GO were also represented in their respective Raman spectra in Figure 7 [52].

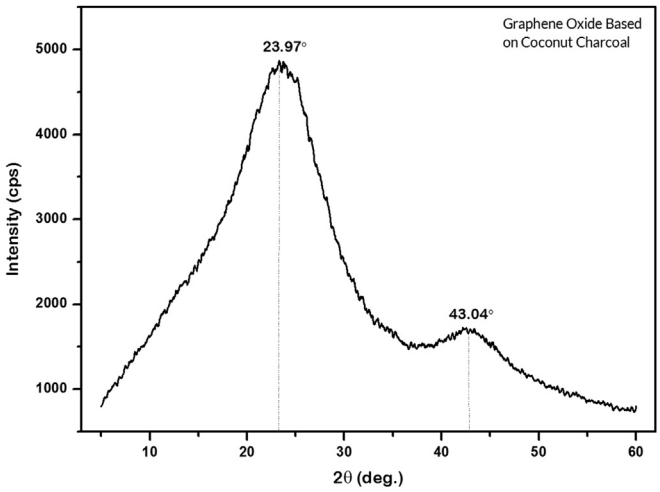

Figure 5. GO diffractogram pattern based on the coconut shell waste.

In a carbonaceous material, the D band and G band correspond to the spa^{2}and sp^3 carbon stretching types and their intensity ratio (I_D/I_G) is used as a measure of the amount of disorder present within the carbon materials [24]. The Raman spectrum of GO was identified by first-order scattering of the E_{2g} phonon from the sp^2 C atoms that caused the G mode to appear (~1595 cm^{-1}) and a breathing mode of the k-point photons of the A_{1g} symmetry. Moreover, a defect from the sample caused the D mode to appear (~1355.5 cm^{-1}). For samples with good quality, the value of the I_D/I_G intensity ratio is less than 2 [53], and the GO-based coconut shell waste has the I_D/I_G intensity ratio of 0.89. The observed results strongly indicate the similarities I_D/I_G intensity ratio with that reported by Simon *et al.* [27], and Kim *et al.*, [54]. The 2D band is a crucial parameter for determining the formation or layer totals of the GO

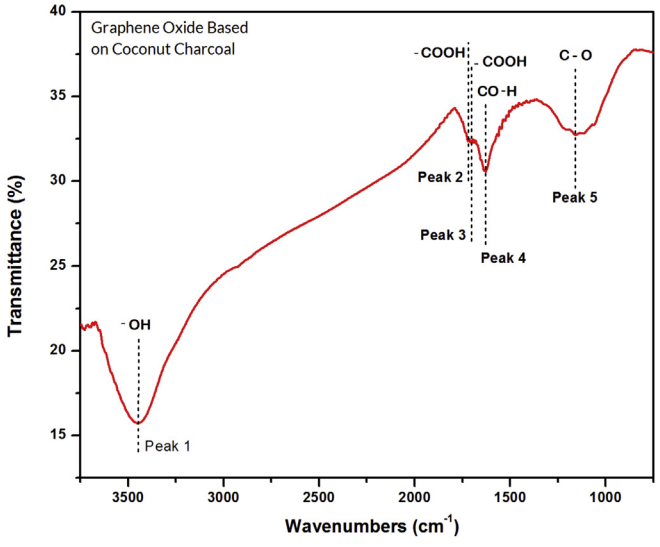

Figure 6. FTIR spectrum of GO-based on coconut shell waste.

Table 3. Microstructural XRD data of the three highest peaks of graphite sample based on coconut shell waste.

No.	Peak no.	Two thetas (deg)	d (Å)	In/I1 (%)	FWHM (deg)	Intensity (Counts)	Integrated Int (Counts)
1	36	44.0462	2.05424	100	0.18530	1312	13895
2	33	39.5240	2.27823	30	0.15370	395	3505
3	32	37.8129	2.37729	20	0.19240	258	3314

Table 4. Bond types (functional groups) and wavenumber of GO materials.

Peak	Wavenumber (GO-based Coconut Shell Waste) (cm^{-1})	Bond types (Functional groups)	Wavenumber (GO-based commercial graphite) (cm^{-1})	Bond types (Functional groups)
1	3449.92	-OH (Hydroxyl) stretching	3427	-OH (Hydroxyl) stretching
2	1719.42	-COOH (Carboxyl) stretching	1730	-COOH (Carboxyl) stretching
3	1702.62	-COOH (Carboxyl) stretching	1630	C–OH (Alcohol) stretching
4	1628.12	C–OH (Alcohol) stretching	1371	C–OH (Alcohol) stretching
5	1158.51	C–O (Epoxy) stretching	1054	C–O (Epoxy) stretching

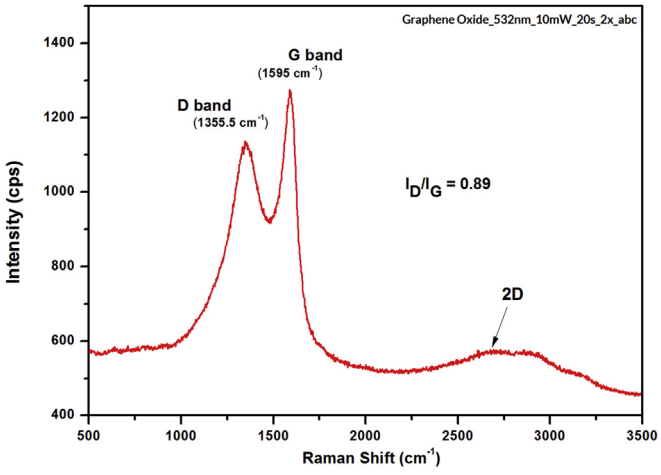

Figure 7. Raman spectra of GO-based on coconut shell waste.

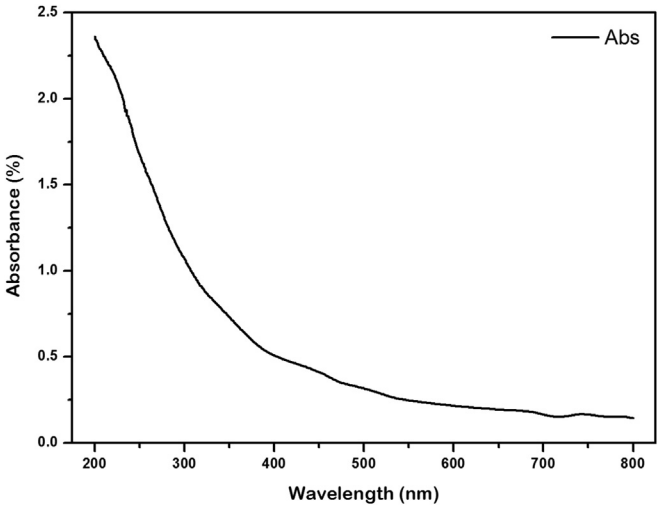

Figure 8. UV-Visible spectrum of GO-based on coconut shell waste.

sample [9]. For the GO sample, the 2D band peak position at ~2668 cm^{-1}confirmed the single presence layer.

3.5. UV-visible analysis

UV-Visible characterization was used to determine the optical properties of the GO-based coconut shell waste [55]. The absorbance spectrum given in Figure 8 shows the value of the intensity of light or energy absorbed by the particles in a colloidal solution of GO sample-based coconut shell waste in the wavelength range of 200-800 nm that indicates the optical properties of the material. Then, the UV-Vis spectrum results were analysed using the Tauc plot method in order to determine the bandgap energy values of the GO material [56, 57]. Equation (1) determines the bandgap energy as:

$$(\alpha h\nu)^2 = K(h\nu - Eg) \quad (1)$$

where α is the absorption coefficient, $h\nu$ is the photon energy, K is the energy-independent constant, and Eg is the bandgap [58]. The value of $h\nu$ is 1240 as obtained from the Planck equation. Subsequently, the value of α is 2.303 as calculated from the absorbance data using the Beer--Lamberts' Law, as illustrated in Figure 9. The absorbance is given by (2):

$$\alpha = A\frac{1}{\log(e)L} \quad (2)$$

Where A is the absorbance data, $\log(e)$ is 0.4343, and L is the cuvette path length (1 cm). The values of Eg are equal to the intercept on the abscissa obtained by fitting of the Tauc equation $(\alpha h\nu)^2 \sim h\nu$ plots [58]. The results of bandgap energy analysis using the Tauc plot method of GO-based coconut shell waste are shown in Figure 10. The study shows that the value of

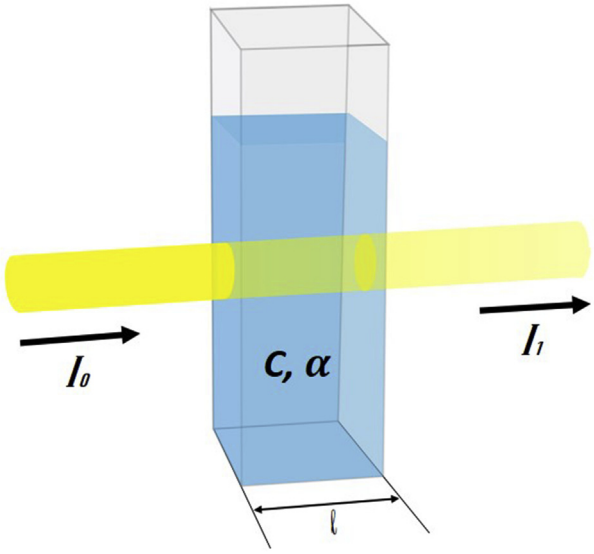

Figure 9. Schematic of Beer Lambert's law.

the band gap energy of GO was 4.38 eV. This result indicates that coconut shell waste that is initially present as an insulator material [59], whereas the insulator has the band gap energy ≥5 eV and after synthesized into GO material, is a semiconductor with a bandgap energy <5 eV [60]. The bandgap energy-reduction was due to the exfoliation of graphite powder and the sonication of the sample during the synthesis process [22]. This

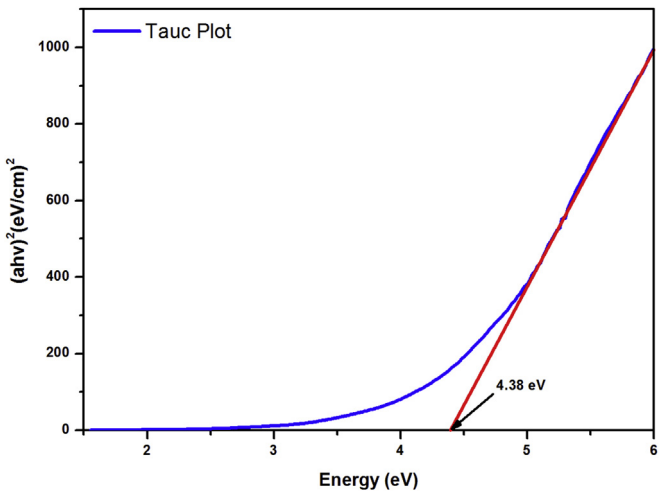

Figure 10. Bandgap energy of GO-based on the coconut shell waste after analysis using the Tauc plot method.

result was also related to several previous studies where we can adjust the optical properties of GO by varying the oxidation level [2].

4. Conclusions

AGO material has was successfully synthesized from coconut shell waste by a modified Hummers method. The XRD results showed that 71.53% of graphite 2H observed with GO sample tended to form a rGO phase. Meanwhile, FTIR spectroscopy confirmed the appearance of various oxygen-containing functional groups such as hydroxyl, carboxyl, alcohol, and epoxy within the GO structure. The value of the I_D/I_G intensity ratio of the GO sample was 0.89 with a 2D single layer and had a surface morphology with an abundance of granular particles with different size distributions. The analysis using the Tauc plot method shows that the value of the GO band gap energy was 4.38 eV, indicating its semiconductor properties.

Declarations

Author contribution statement

Eko H. Sujiono: Conceived and designed the experiments; Analyzed and interpreted the data; Contributed reagents, materials, analysis tools or data; Wrote the paper.

Zurnansyah Z., Dirfan Zabrian: Performed the experiments; Contributed reagents, materials, analysis tools or data.

Muhammad Y. Dahlan, Bunga D. Amin: Analyzed and interpreted the data; Contributed reagents, materials, analysis tools or data.

Samnur S.: Contributed reagents, materials, analysis tools or data; Wrote the paper.

Jasdar Agus: Conceived and designed the experiments; Performed the experiments.

Funding statement

This work was supported by the Universitas Negeri Makassar Research Institution, a research scheme of PNBP, acceleration of professorships program (1380/UN36.9/PL/2019) and the fundamental research program, Ministry Research and Technology, Republic of Indonesia.

Competing interest statement

The authors declare no conflict of interest.

Additional information

No additional information is available for this paper.

References

[1] S.N. Alam, N. Sharma, L. Kumar, Synthesis of graphene oxide (GO) by modified Hummers method and its thermal reduction to obtain reduced graphene oxide (rGO), Graphene 6 (1) (2017) 1–18.
[2] J. Guerrero-Contreras, F. Caballero-Briones, Graphene oxide powders with different oxidation degree, prepared by synthesis variations of the Hummers method, Mater. Chem. Phys. 153 (Mar. 2015) 209–220.
[3] C. Zhang, et al., Graphene oxide reduced and modified by environmentally friendly glycylglycine and its excellent catalytic performance, Nanotechnology 25 (13) (Apr. 2014) 135707.
[4] J.C. Meyer, A.K. Geim, M.I. Katsnelson, K.S. Novoselov, T.J. Booth, S. Roth, The structure of suspended graphene sheets, Nature 446 (7131) (Mar. 2007) 60–63.
[5] S. Stankovich, et al., Graphene-based composite materials, Nature 442 (7100) (Jul. 2006) 282–286.
[6] H.B. Heersche, P. Jarillo-Herrero, J.B. Oostinga, L.M.K. Vandersypen, A.F. Morpurgo, Bipolar supercurrent in graphene, Nature 446 (7131) (Mar. 2007) 56–59.
[7] A.A. Balandin, et al., Superior thermal conductivity of single-layer graphene, Nano Lett. 8 (3) (Mar. 2008) 902–907.
[8] al. Rattanaet, Preparation and characterization of graphene oxide nanosheets, Procedia Eng. 32 (2012) 759–764.
[9] Y.H. Ding, P. Zhang, Q. Zhuo, H.M. Ren, Z.M. Yang, Y. Jiang, A green approach to the synthesis of reduced graphene oxide nanosheets under UV irradiation, Nanotechnology 22 (21) (May 2011) 215601.
[10] G.K. Ramesha, A. Vijaya Kumara, H.B. Muralidhara, S. Sampath, Graphene and graphene oxide as effective adsorbents toward anionic and cationic dyes, J. Colloid Interface Sci. 361 (1) (Sep. 2011) 270–277.
[11] J. Song, X. Wang, C.-T. Chang, Preparation and characterization of graphene oxide, J. Nanomater. 2014 (2014) 1–6.
[12] Q. Zheng, Z. Li, J. Yang, J.-K. Kim, Graphene oxide-based transparent conductive films, Prog. Mater. Sci. 64 (Jul. 2014) 200–247.
[13] X. Huang, et al., Graphene-based materials: synthesis, characterization, properties, and applications, Small 7 (14) (Jul. 2011) 1876–1902.
[14] T. Guo, X. Chen, L. Su, C. Li, X. Huang, X.-Z. Tang, "Stretched graphene nanosheets formed the 'obstacle walls' in melamine sponge towards effective electromagnetic interference shielding applications, Mater. Des. 182 (Nov. 2019) 108029.
[15] J. Luo, J. Wang, F. Xia, X. Huang, Direct growth of large area uniform double layer graphene films on MgO(100) substrates by chemical vapor deposition, Mater. Chem. Phys. 233 (May 2019) 213–219.
[16] A. Cinar, S. Baskut, A.T. Seyhan, S. Turan, Tailoring the properties of spark plasma sintered SiAlON containing graphene nanoplatelets by using different exfoliation and size reduction techniques: anisotropic mechanical and thermal properties, J. Eur. Ceram. Soc. 38 (4) (Apr. 2018) 1299–1310.
[17] S. Gurunathan, J. Woong Han, V. Eppakayala, J. Kim, Green synthesis of graphene and its cytotoxic effects in human breast cancer cells, Int. J. Nanomed. 1015 (Mar. 2013).
[18] G. Shao, Y. Lu, F. Wu, C. Yang, F. Zeng, Q. Wu, Graphene oxide: the mechanisms of oxidation and exfoliation, J. Mater. Sci. 47 (10) (May 2012) 4400–4409.
[19] X. Li, et al., "Highly conducting graphene sheets and Langmuir–Blodgett films, Nat. Nanotechnol. 3 (9) (Sep. 2008) 538–542.
[20] Q. Liu, Y. Gong, T. Wang, W.-L. Chan, J. Wu, Metal-catalyst-free and controllable growth of high-quality monolayer and AB-stacked bilayer graphene on silicon dioxide, Carbon 96 (Jan. 2016) 203–211.
[21] G. Eda, C. Mattevi, H. Yamaguchi, H. Kim, M. Chhowalla, Insulator to semimetal transition in graphene oxide, J. Phys. Chem. C 113 (35) (Sep. 2009) 15768–15771.
[22] H. Yu, B. Zhang, C. Bulin, R. Li, R. Xing, High-efficient synthesis of graphene oxide based on improved Hummers method, Sci. Rep. 6 (1) (Dec. 2016).
[23] W.S. Hummers, R.E. Offeman, Preparation of graphitic oxide, J. Am. Chem. Soc. 80 (6) (Mar. 1958) 1339, 1339.
[24] J. Chen, Y. Li, L. Huang, C. Li, G. Shi, High-yield preparation of graphene oxide from small graphite flakes via an improved Hummers method with a simple purification process, Carbon 81 (Jan. 2015) 826–834.
[25] J. Wang, et al., Ultra-thin, highly graphitized carbon nanosheets into three-dimensional interconnected framework utilizing a ball mill mixing of precursors, Chem. Eng. J. 374 (Oct. 2019) 1214–1220.
[26] Q. Yang, et al., "Effect of environmental regulations on China's graphite export, J. Clean. Prod. 161 (Sep. 2017) 327–334.
[27] M. Simón, A. Benítez, A. Caballero, J. Morales, O. Vargas, Untreated natural graphite as a graphene source for high-performance Li-ion batteries, Batter. 4 (1) (Mar. 2018) 13.
[28] F.M. Wachid, A.Y. Perkasa, F.A. Prasetya, N. Rosyidah, Darminto, "Synthesis and Characterization of Nanocrystalline Graphite from Coconut Shell with Heating Process," Presented at the 5th Nanoscience and Nanotechnology Symposium (Nns2013), Surabaya, Indonesia, 2014, pp. 202–206.
[29] A.K. Bledzki, A.A. Mamun, J. Volk, Barley husk and coconut shell reinforced polypropylene composites: the effect of fibre physical, chemical and surface properties, Compos. Sci. Technol. 70 (5) (May 2010) 840–846.
[30] T. Kim, C. Jo, W.-G. Lim, J. Lee, J. Lee, K.-H. Lee, Facile conversion of activated carbon to battery anode material using microwave graphitization, Carbon 104 (Aug. 2016) 106–111.

[31] I. Made Joni, M. Vanitha, P. Camellia, N. Balasubramanian, Augmentation of graphite purity from mineral resources and enhancing % graphitization using microwave irradiation: XRD and Raman studies, Diam. Relat. Mater. 88 (Sep. 2018) 129–136.
[32] A. Nicholas, M. Hussein, Z. Zainal, T. Khadiran, Palm Kernel shell activated carbon as an inorganic framework for shape-stabilized phase change material, Nanomaterials 8 (9) (Sep. 2018) 689.
[33] G. Zhang, Y. Chen, Y. Chen, H. Guo, Activated biomass carbon made from bamboo as electrode material for supercapacitors, Mater. Res. Bull. 102 (Jun. 2018) 391–398.
[34] N.K. Rukman, M. Jannatin, G. Supriyanto, M.Z. Fahmi, W.A.W. Ibrahim, GO-Fe3O4 Nanocomposite from coconut shell: synthesis and characterization, IOP Conf. Ser. Earth Environ. Sci. 217 (Jan. 2019), 012008.
[35] Y. Park, S. Hyun, M. Chun, Grain size effect on mechanical properties of polycrystalline graphene, Compos. Res. 29 (6) (Dec. 2016) 375–378.
[36] M.Q. Chen, S.S. Quek, Z.D. Sha, C.H. Chiu, Q.X. Pei, Y.W. Zhang, "Effects of grain size, temperature and strain rate on the mechanical properties of polycrystalline graphene – a molecular dynamics study, Carbon 85 (Apr. 2015) 135–146.
[37] J. Du, H.-M. Cheng, The fabrication, properties, and uses of graphene/polymer composites, Macromol. Chem. Phys. 213 (10–11) (Jun. 2012) 1060–1077.
[38] L. Kittiratanawasin, S. Hannongbua, The effect of edges and shapes on band gap energy in graphene quantum dots, Integr. Ferroelectr. 175 (1) (Oct. 2016) 211–219.
[39] J. Tian, V. Miller, P.C. Chiu, J.A. Maresca, M. Guo, P.T. Imhoff, Nutrient release and ammonium sorption by poultry litter and wood biochars in stormwater treatment, Sci. Total Environ. 553 (May 2016) 596–606.
[40] L. Wang, L. Wang, W. He, L. An, S. Xu, Nutrient resorption or accumulation of desert plants with contrasting sodium regulation strategies, Sci. Rep. 7 (1) (Dec. 2017) 17035.
[41] Y. Cai, H. Chen, R. Yuan, F. Wang, Z. Chen, B. Zhou, Toxicity of perfluorinated compounds to soil microbial activity: effect of carbon chain length, functional group and soil properties, Sci. Total Environ. 690 (Nov. 2019) 1162–1169.
[42] D. Ge, J. Shi, Y. Zhang, L. Zhang, P. Yang, Numerical simulation of a novel bilayer photonic crystal slab biosensor with hexagonal lattice, Results Phys. 12 (Mar. 2019) 1942–1945.
[43] G. Liu, L. Wang, B. Wang, T. Gao, D. Wang, A reduce graphene oxide modified metallic cobalt composite with superior electrochemical performance for supercapacitors, RSC Adv. (2015) 10.
[44] L. Guo, et al., Reduced graphene oxide/α-Fe 2 O 3 composite nanofibers for application in gas sensors, Sensor. Actuator. B Chem. 244 (Jun. 2017) 233–242.
[45] O.C. Compton, S.T. Nguyen, Graphene oxide, highly reduced graphene oxide, and graphene: versatile building blocks for carbon-based materials, Small 6 (6) (Mar. 2010) 711–723.
[46] Md.S.A. Sher Shah, A.R. Park, K. Zhang, J.H. Park, P.J. Yoo, "Green synthesis of biphasic TiO2 –reduced graphene oxide nanocomposites with highly enhanced photocatalytic activity, ACS Appl. Mater. Interfaces 4 (8) (Aug. 2012) 3893–3901.
[47] P. Khanra, C.-N. Lee, T. Kuila, N.H. Kim, M.J. Park, J.H. Lee, 7,7,8,8-Tetracyanoquinodimethane-assisted one-step electrochemical exfoliation of graphite and its performance as an electrode material, Nanoscale 6 (9) (2014) 4864–4873.
[48] R.K. Singh, R. Kumar, D.P. Singh, Graphene oxide: strategies for synthesis, reduction and frontier applications, RSC Adv. 6 (69) (2016) 64993–65011.
[49] C. Monteserín, et al., Effects of graphene oxide and chemically-reduced graphene oxide on the dynamic mechanical properties of epoxy amine composites, Polymers 9 (12) (Sep. 2017) 449.
[50] Yunhe Xu, Jun Li, Wenxin Huang, Porous graphene oxide prepared on nickel foam by electrophoretic deposition and thermal reduction as high-performance supercapacitor electrodes, Materials 10 (8) (Aug. 2017) 936.
[51] H.-L. Guo, X.-F. Wang, Q.-Y. Qian, F.-B. Wang, X.-H. Xia, A green approach to the synthesis of graphene nanosheets, ACS Nano 3 (9) (Sep. 2009) 2653–2659.
[52] M. Bera, Chandravati, P. Gupta, P.K. Maji, Facile one-pot synthesis of graphene oxide by sonication assisted mechanochemical approach and its surface chemistry, J. Nanosci. Nanotechnol. 18 (2) (Feb. 2018) 902–912.
[53] A. Kaniyoor, S. Ramaprabhu, A Raman spectroscopic investigation of graphite oxide derived graphene, AIP Adv. 2 (3) (Sep. 2012), 032183.
[54] S.-G. Kim, O.-K. Park, J.H. Lee, B.-C. Ku, Layer-by-layer assembled graphene oxide films and barrier properties of thermally reduced graphene oxide membranes, Carbon Lett. 14 (4) (Oct. 2013) 247–250.
[55] M. Hasani, M. Mahdavian, H. Yari, B. Ramezanzadeh, Versatile protection of exterior coatings by the aid of graphene oxide nano-sheets; comparison with conventional UV absorbers, Prog. Org. Coating 116 (Mar. 2018) 90–101.
[56] A. Dolgonos, T.O. Mason, K.R. Poeppelmeier, Direct optical band gap measurement in polycrystalline semiconductors: a critical look at the Tauc method, J. Solid State Chem. 240 (Aug. 2016) 43–48.
[57] B.D. Viezbicke, S. Patel, B.E. Davis, D.P. Birnie, Evaluation of the Tauc method for optical absorption edge determination: ZnO thin films as a model system: Tauc method for optical absorption edge determination, Phys. Status Solidi B 252 (8) (Aug. 2015) 1700–1710.
[58] F. Zheng, W.-L. Xu, H.-D. Jin, X.-T. Hao, K.P. Ghiggino, Charge transfer from poly (3-hexylthiophene) to graphene oxide and reduced graphene oxide, RSC Adv. 7 (2015).
[59] T. Saithanu, A. Suksri, Coconut shell powder and electrical tree inhibition of solid insulator, Key Eng. Mater. 775 (Aug. 2018) 89–93.
[60] V. Quaschning, Understanding Renewable Energy Systems, Earthscan, London, 2005, p. 119.